iScience

CellPress
OPEN ACCESS

Review

A review of electrospun metal oxide semiconductor-based photocatalysts

Fushui Guo,[1] Liantao Hao,[1] Liu Feng,[1] Bingjie Hu,[1] Jinye Niu,[1] Xuliang Zhang,[1,2,*] Shuangying Chen,[1,*] and Bo Liu[2,*]
[1]Analysis and Testing Center, Shandong University of Technology, 266 Xincun Xi road, Zibo 255000, P.R. China
[2]Laboratory of Functional Molecules and Materials, School of Physics and Optoelectronic Engineering, Shandong University of Technology, 266 Xincun Xi road, Zibo 255000, P.R. China
*Correspondence: zhangxl@sdut.edu.cn (X.Z.), chen05537@qq.com (S.C.), liub@sdut.edu.cn (B.L.)
https://doi.org/10.1016/j.isci.2024.111675

SUMMARY

In recent years, photocatalytic materials with a nanofiber-like morphology have garnered a surge of academic attention due to their distinctive properties, including an expansive specific surface area, a considerable high aspect ratio, a pronounced resistance to agglomeration, superior electron survivability, and robust surface activity. Consequently, the synthesis of photocatalytic nanofiber materials through various methodologies has drawn considerable attention. The electrospinning technique has been established as a prevalent method for fabricating nanofiber-structured materials, owing to its advantageous properties, including the ability for mass production and the assurance of high continuity. This review focuses on metal oxide semiconductor-based materials, which are crucial components of photocatalysts. We summarize several recent studies that explore morphology modulation, surface modification, element doping, and composite construction using uniaxial and coaxial electrospinning techniques. Finally, we present potential approaches for constructing high-activity photocatalytic systems through electrospinning technique.

INTRODUCTION

Historically, the earliest catalysts consisted of three-dimensional bulk materials or particle-like structures, typically composed of metals, oxides, or other active substances in a solid state. Although these materials demonstrated certain catalytic capabilities, they were inherently limited by their large particle size and restricted surface area, constraining their catalytic activity and selectivity.[1] To overcome these issues, research has increasingly focused on modulating catalyst morphology—by reducing particle size, developing two-dimensional sheets, and creating one-dimensional nanostructures like nanofibers.[2–4] One-dimensional nanofibers and nanowires, with their high surface area-to-volume ratios arising from their extreme extensiveness in one dimension and thinness in the other two dimensions, have shown remarkable potential in improving catalyst performance by enhancing selectivity, reducing side reactions, and promoting efficient electron transport.[5] Consequently, the synthesis of photocatalytic nanofiber materials has attracted considerable attention due to their unique properties, including extensive specific surface area, high aspect ratios, significant resistance to agglomeration, enhanced electron survivability, and robust surface activity, and related works have thus been widely researched to facilitate the exploration of diverse methodologies aimed at optimizing their production.[6]

Among the various techniques for preparing one-dimensional nanofibers, such as templating, sol-gel, and self-assembly, electrospinning stands out due to its unique advantages, including the ability to modulate the specific surface area of the material, feasibility for mass production, and simplicity of the apparatus, which requires only a syringe, a receiver, and a high-voltage power supply, as shown in Figure 1.[7,8]

The electrospinning technique does not require complex equipment or substantial expense, yet it facilitates the rapid generation of nanofibers within a short time frame, simultaneously ensuring that the fibers exhibit an exceptionally high surface area-to-volume ratio, thus guaranteeing its practicability and scalability. Electrospinning is rapidly differentiating from the single-fluid electrospinning to bi-fluid coaxial and side-by-side electrospinning, and to tri-fluid coaxial, Janus, and their combined electrospinning processes.[9–14] Meanwhile, electrospinning is also frequently combined with other traditional techniques such as electrospraying and solvent casting for expanding its capability of creating nanofibers.[15–17] However, the most popular electrospinning processes are uniaxial and coaxial processes, as shown in Figure 2, which have been broadly employed for producing metal oxide semiconductor-based photocatalysts. Relatively speaking, uniaxial electrospinning is limited in producing more complex structures when compared with the coaxial electrospinning. When compared with uniaxial electrostatic spinning, the most notable distinction is that the coaxial needle comprises two parts. One part of the apparatus is loaded with the shell liquid, whereas the other part is loaded with the core liquid. On the other hand, to construct photocatalytic systems with enhanced activities, many modulation strategies have been developed, such as surface modification, element doping, and composite construction. By coaxial spinning or adding additional components into the spinning solution,

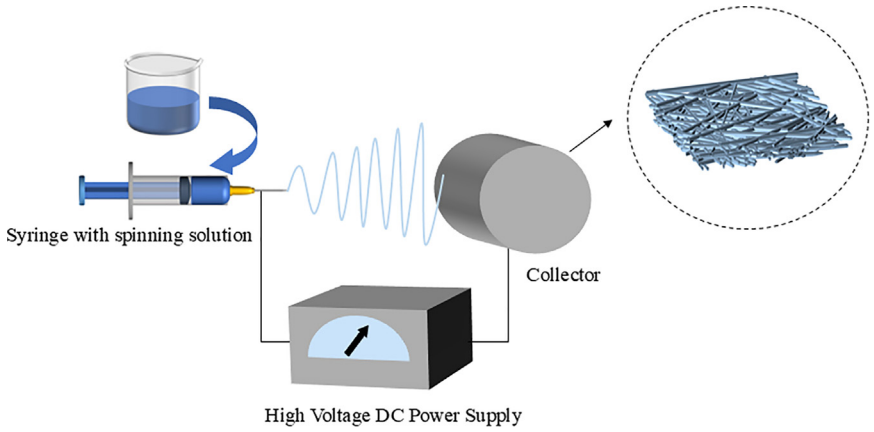

Figure 1. Schematic diagram of the electrospinning device

the above-mentioned modulations can be easily realized through an *in situ* process.[18]

Based on the above investigation, this review provides a systematic survey and summary of current research on the preparation of highly active photocatalytic systems using electrospinning technology, focusing primarily on enlarging the specific surface area of the materials by modulating their morphology, modifying some functional groups or metal particles on their surface, doping some elements in their structure, and introducing other semiconductor materials to construct composites. At last, we propose a promising strategy for constructing photocatalytic systems with enhanced charge separation properties and catalytic performance through coaxial electrospinning technology.

MORPHOLOGY MODULATION

The specific surface area of bulky, large-sized materials is inherently limited, as depicted in Figure 3A, resulting in fewer surface-active sites and reduced contact with reactants. To address this issue, nanofibers produced via electrospinning, as shown in Figure 3B, have been widely researched for their ability to increase the specific surface area.[19] By adjusting parameters such as solution viscosity, voltage, and flow rate, it is possible to create materials with varying pore sizes. Among these techniques, coaxial electrospinning (illustrated in Figure 3C) produces hollow or core-shell fibers, which further enhance performance by increasing surface area and facilitating efficient carrier migration.[20,21] This structure improves charge separation and reduces electron-hole recombination due to shortened migration pathways. Additionally, hollow porous nanofibers, shown in Figure 3D, provide even greater advantages with their porous structure, introducing additional channels and active sites.[22] This configuration promotes reactant diffusion, enhances charge carrier separation, and suppresses electron-hole recombination, resulting in significantly improved photocatalytic efficiency.

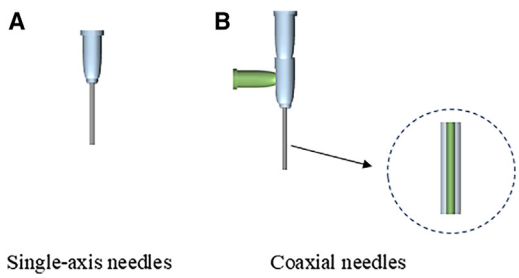

Figure 2. (A and B) Comparison of single-axis and coaxial needles

A number of studies have employed uniaxial electrostatic spinning to fabricate fibrous photocatalysts with a high specific surface area. For example, Juncai Lu et al.[23] prepared $ZnWO_4$ nanofibers using uniaxial electrospinning, achieving a specific surface area of 110 $m^2\ g^{-1}$, which was significantly higher than the 75 $m^2\ g^{-1}$ of irregular $ZnWO_4$ nanoparticles prepared by the same method. This increase in surface area, attributed to the electrospinning process, also led to a higher density of defects and active sites, enhancing the material's catalytic efficiency. As a result, the $ZnWO_4$ nanofibers degraded 70% of RhB (10 mg/L) within 45 min, compared with 70 min required by the nanoparticles. The enhanced surface area and accelerated charge separation due to electrospinning are also crucial for improving hydrogen production technologies.

Ling Wang et al.[24] synthesized $MgTiO_3$ nanofibers with a specific surface area of 22.62 $m^2\ g^{-1}$, about 3.5 times greater than that of $MgTiO_3$ particles (6.3 $m^2\ g^{-1}$) prepared via sol-gel and calcination. The high aspect ratio of the nanofibers enhanced light absorption and facilitated rapid migration of photogenerated charge carriers, reducing electron-hole recombination and improving charge transport. This led to a hydrogen production rate of 0.33 mmol $g^{-1}\cdot h^{-1}$, four times higher than that of $MgTiO_3$ particles. The porous structure between nanofibers further enhanced reactant conversion and hydrogen production efficiency.

Shama Perween et al.[25] produced $ZnTiO_3$ nanopowders via uniaxial electrospinning, starting with calcination to form $ZnTiO_3$ powder, followed by sol formation with a surfactant, and finally electrospinning. The specific surface area of the electrospun $ZnTiO_3$ (24.47 $m^2\ g^{-1}$) was significantly higher than that of the sol-gel-prepared sample (1.05 $m^2\ g^{-1}$). The increased surface area and nanoporous structure, formed by removing organic components during synthesis, contributed to a 1.7-fold improvement in the phenol degradation rate under visible light, showcasing superior photocatalytic performance.

Some studies have utilized coaxial electrospinning to create hollow fiber structures, aiming to further enhance the material's specific surface area. For instance, Juran Kim et al.[26] utilized coaxial electrospinning to fabricate TiO_2 hollow nanofibers, where the transition from solid to hollow structures was controlled by varying the core solution flow rate. When the flow rate was set

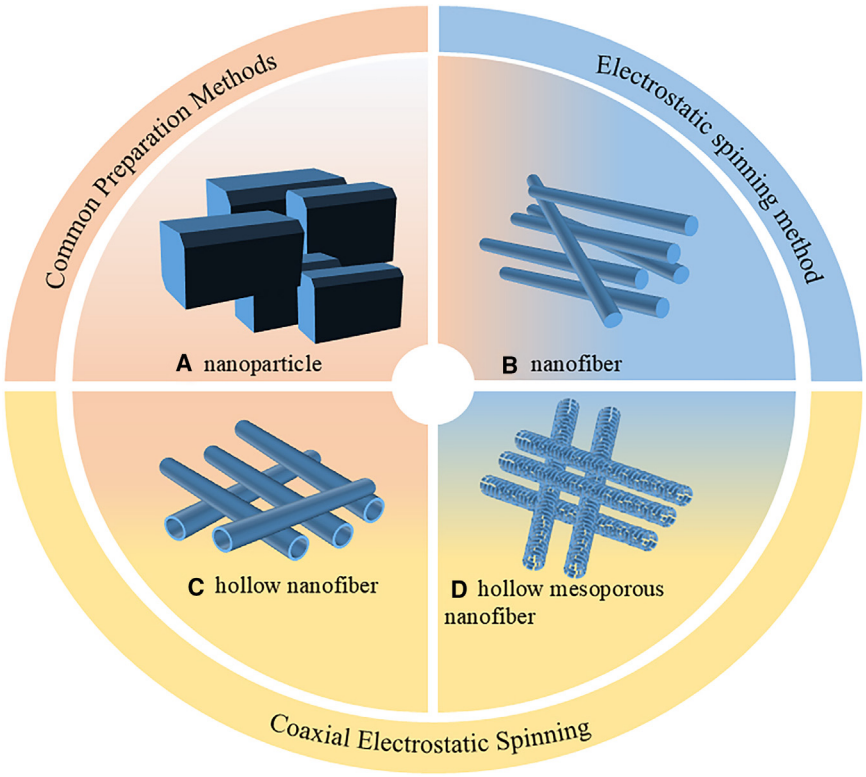

Figure 3. Comparison of the different morphology, including nanoparticle from common preparation methods (A), nanofiber (B), hollow nanofiber (C) and hollow mesoporous nanofiber (D) from electrospinning method.

to zero, the resulting solid fibers had a specific surface area of 16.01 m^2 g^{-1}, comparable to fibers produced by uniaxial spinning. However, as the core solution flow increased, the fibers transformed into hollow nanofibers, achieving a maximum surface area of 51.28 m^2 g^{-1}. This hollow architecture, characterized by a larger internal cavity, significantly increased the material's surface active sites, thereby enhancing its adsorption capacity and catalytic performance. The unique layered structure also facilitated greater exposure of catalytic sites to reactants, allowing for more efficient diffusion and interaction. As a result, the NO removal rate within 60 min reached 66.2%, more than double the 31.2% achieved by the solid fibers. This improvement is largely due to the increased surface area and improved electron transport across the hollow structure, which enhances the availability of reactive species at the active sites.

Shudan Li et al.[27] employed a similar coaxial electrospinning method, using air as the core material to produce hollow, mesoporous $LaFeO_3$ nanofibers with a belt-like structure. The hollow fibers, with their high porosity, differed markedly from the densely packed uniaxial fibers typically formed after calcination. The hollow structure not only provided a larger surface area but also improved light utilization by enhancing the penetration and scattering of light within the fiber matrix, increasing the efficiency of photocatalytic reactions. Moreover, the belt-like structure of the nanofibers facilitated greater contact between the catalyst and the reaction substrate, improving mass transfer. The smaller crystalline domains further contributed to the reduction of photogenerated electron-hole recombination by shortening the distance electrons and holes must travel to reach the surface, thus optimizing the photocatalytic activity. These structural advantages resulted in a methylene blue (MB) degradation efficiency of 59.79% within 2 h, demonstrating the efficacy of hollow, mesoporous fibers in enhancing both light absorption and catalytic performance.

Both uniaxial electrostatic spinning and coaxial electrostatic spinning are feasible methods in regulating the morphology of materials, thereby enhancing their specific surface area. Herein, a summary of some related works is presented as shown in Table 1, including the related spinning conditions, carrier polymers used, and catalytic efficiency.

SURFACE MODIFICATION

Surface modification of groups, molecules, or metal particles is a widely used method for enhancing charge separation, light absorption, or redox capacity of photocatalysts.[31] As illustrated in Figure 4, introducing raw materials into the spinning solution is a feasible method for surface modification.[32,33] Besides, in the postmodification method, the fiber-like structure of the catalyst prevents agglomeration, which is also beneficial for subsequent modifications.

Several studies have demonstrated the critical role of electrospinning in tailoring photocatalytic materials by facilitating the incorporation and precise distribution of modifying agents during synthesis. For instance, Chunqie Han and colleagues[34] synthesized Ag/Ga_2O_3 photocatalysts using electrospinning, introducing Ag nanoparticles via *in situ* surface modification. Although the specific surface area decreased from 19.6 m^2/g (pure Ga_2O_3) to 14.3 m^2/g (Ag/Ga_2O_3), the photocatalytic hydrogen production increased 6-fold. This improvement was driven by the structural benefits from electrospinning, which ensured uniform Ag nanoparticle distribution, enhancing charge separation and reducing electron-hole recombination. Additionally, the plasmonic effects of Ag nanoparticles expanded light absorption into the visible spectrum, compensating for the reduced surface area and boosting photocatalytic activity.

Similarly, Ye Shengjun et al.[35] used electrospinning to incorporate multi-walled carbon nanotubes (MWCNTs) into BiVO4 nanofibers. The MWCNTs formed a conductive network that enhanced electron mobility and minimized recombination. Although surface area data were not provided, the structural changes reduced the band gap from 2.35 to 2.16 eV, leading to improved visible light absorption and a 2-fold increase in the photocatalytic degradation of oxytetracycline.

Table 1. Morphological modulation using electrostatic spinning

Photocatalyst	Spinning conditions	Solvents	Carrier polymers	Photocatalytic testing	Test conditions	Activity results	Reference
$ZnWO_4$	Voltage 15 kV Distance (to needle tip) 15 cm	DI	PVP	Degrading RhB	RhB solution at 10 mg/L	70% within 45 min	Lu et al.[23]
$MgTiO_3$	Voltage 12 kV Distance 12 cm	CH_3COOH, CH_3OH	PVP	Hydrogen production	300-W Xe lamp	0.33 mmol $g^{-1}\cdot h^{-1}$	Wang et al.[24]
$ZnTiO_3$	Voltage 10 kV Distance 12 cm	CH_3COOH	PVA	Degrading C_6H_6O	Visible light (output power 100 W)	70% within 1 h	Perween et al.[25]
TiO_2	Voltage 15 kV Distance 12 cm	DMF, CH_3COOH, C_2H_5OH	PVP	Degrading RhB	200-W Xe light RhB solution at 20 mg/L	99% within 90 min	Kim et al.[26]
$LaFeO_3$	Pushing speed 0.4 mL h−1 Distance 12 cm	CH_3COOH, C_2H_5OH	PVP	Degrading MB	125-W Xe light MB solution at 5 mg/L	59.8% within 120 min	Li et al.[27]
BiVO4	Voltage 16 kV Distance 14 cm	DMF, CH_3COOH, C_2H_5OH	PVP	Redox Cr(VI)	Cr(VI) solution concentration 10 mg/L	95.3% within 80 min	Lv et al.[28]
ZnO	Voltage 17 kV Distance 11 cm	DMF	PAN	Degrading MB	MB solution concentration 15 μM	99% within 60 min	Pantò et al.[29]
WO_3	Voltage 28 kV Distance 15 cm	DMF, C_2H_5OH	PVP	Degrading C_6H_6O	C_6H_6O solution at 20 mg/L	2.87 mg L−1·h−1	Tong et al.[30]

DI, deionized water; PVP, polyvinyl pyrrolidone; PVA, polyvinyl alcohol; PAN, polyacrylonitrile; DMF, dimethyl formamide.

Seonyoung Jo and colleagues[36] applied electrospinning to create TiO_2 nanofibers modified with perovskite quantum dots (PQDs). The resulting mesoporous structure increased the interaction surface with water, improving hydrophilicity. The uniform distribution of PQDs broadened the light absorption spectrum and improved charge separation, resulting in over 90% degradation of rhodamine B in 1 h, far outperforming commercial TiO_2 (P25).

Several studies have effectively demonstrated the advantages of coaxial electrospinning in enhancing the photocatalytic properties of materials by encapsulating functional modifiers within the outer or inner layers of host nanofibers, as illustrated in Figure 5. For instance, Labeesh Kumar et al.[37] used coaxial electrospinning to fabricate hollow Au@TiO_2 porous nanofibers with gold nanoparticles encapsulated inside. The porous and hollow structure, created by electrospinning, allowed the catalytic sites (Au nanoparticles) to remain highly active while being protected by the TiO_2 shell. Even though the surface area after calcination did not increase dramatically, the hollow structure ensured that the majority of catalytic sites remained accessible, leading to excellent catalytic efficiency and recyclability for the reduction of 4-nitrophenol and Congo red dye.

Similarly, Xiangqian Guo et al.[38] used coaxial electrospinning to synthesize Cu-loaded $SrTiO_3$ nanofibers aimed at enhancing the photocatalytic reduction of CO_2 to CH_3OH. The electrospinning technique facilitated a uniform distribution of Cu across the nanofibers, improving charge separation and electron transfer from $SrTiO_3$ to Cu. Despite the surface area remaining around 10 m^2/g, one-dimensional structure and surface modification with Cu significantly enhanced the photocatalytic efficiency. The methanol yield peaked at 8.08 μmol/g/h when 8% Cu was incorporated, highlighting how electrospinning improved charge dynamics and stability, compensating for the relatively low surface area.

Ruyi Xie et al.[39] employed coaxial electrospinning to fabricate flexible CQDs-$Bi_{20}TiO_{32}$/PAN nanofiber membranes. The CQDs-$Bi_{20}TiO_{32}$ were uniformly anchored to the nanofiber surfaces, while the PAN fibers provided flexibility. Although the surface area increased only modestly (from 7.53 m^2/g to 11.18 m^2/g), the hierarchical structure of the electrospun fibers, with both macro- and mesoporous features, boosted photocatalytic activity, enabling effective degradation of the herbicide isoproturon under visible light. The robust structure also enhanced the catalyst's recyclability and durability, critical for environmental remediation applications.

Electrospinning plays a very important role in the surface modification of materials. Both uniaxial and coaxial electrospinning can prepare materials simply and quickly, greatly improving the efficiency of material synthesis. In particular, coaxial electrospinning technology can precisely encapsulate the surface of materials. To summarize the application of electrospinning in surface modification, we have compiled some research and listed it in Table 2.

ELEMENT DOPING

Modulating the structure of the materials through doping element is also a feasible approach for improving their photocatalytic activities as the dopants can introduce some good

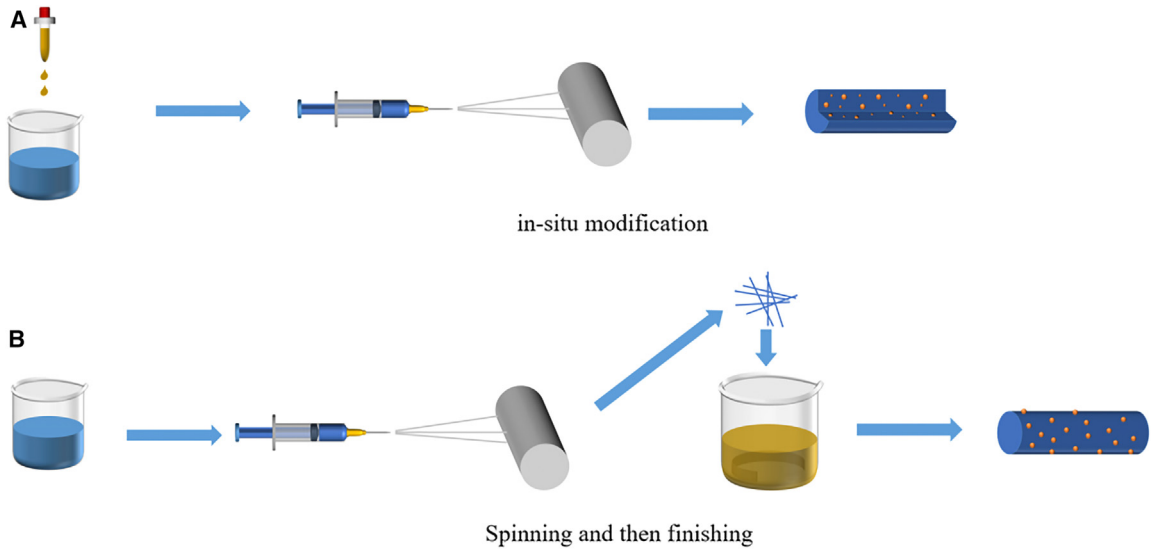

Figure 4. (A and B) Material surface modification methods

properties, including promoting charge separation, providing activity cites, and extending light absorption.[43,44]

Several studies have demonstrated the successful *in situ* doping of nanofibers by introducing a doping source into the spinning solution, followed by electrostatic spinning to create doped nanostructures with enhanced photocatalytic properties.[45] The use of electrospinning, whether uniaxial or coaxial, allows for precise control over the incorporation of dopants, leading to improved material properties such as increased surface area, extended light absorption, and enhanced charge carrier dynamics. For instance, Shaoju Jian et al.[46] fabricated La-doped ZnO nanofibers using electrospinning, achieving 94.31% degradation efficiency for rhodamine B under visible light. La doping introduced oxygen vacancies, improving charge separation and extending the material's light absorption into the visible spectrum. The high surface area and porosity of the electrospun nanofibers enhanced pollutant interaction, reducing recombination and boosting overall photocatalytic performance.

Yan Chen et al.[47] synthesized (N,F)-co-doped $TiO_{2-\delta}$ nanofibers via electrospinning, achieving a specific surface area of 24.27 m_2/g, nearly three times that of commercial TiO_2. The electrospinning technique allowed the formation of mesoporous nanofibers, enhancing both light absorption and charge separation. Nitrogen and fluorine doping introduced oxygen vacancies, crucial for extending light absorption into the visible spectrum and improving electron-hole separation, thus preventing

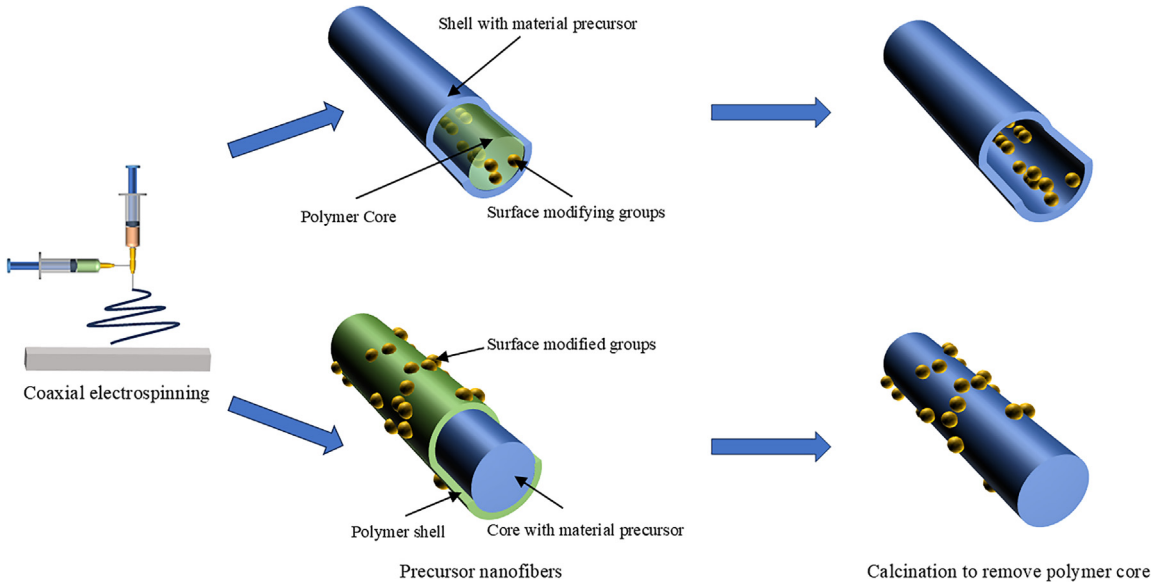

Figure 5. Surface modification structure of coaxial spinning material

Table 2. Surface modification using electrostatic spinning

Photocatalyst	Spinning conditions	Solvents	Carrier polymers	Photocatalytic testing	Test conditions	Activity results	Reference
Ag/Ga_2O_3	Voltage +19, −6 kV	C_2H_5OH	PVP	Hydrogen production	300-W Xe light	65.7 mmol within 2 h	Han et al.[34]
$MWCNT/BiVO_4$	Voltage 15–20 kV Distance 10–15 cm	C_2H_5OH	PVP	Degrading OTC	500-W Xe light OTC solution at 10 mg/L	88.8% within 60 min	Ye et al.[35]
PQDs-modified TiO_2	Voltage 13 kV Distance 12 cm	C_2H_5OH	PVP	Degrading RhB	RhB solution at 20 ppm	97.9% within 2 h	Jo et al.[36]
Au/TiO_2	Voltage 25 kV Distance 20 cm	DMF	PVP	Borohydride reduction of 4-NP	4-NP solution at 0.2 mM	99% within 20 min	Kumar et al.[37]
Cu-loaded $SrTiO_3$	Voltage +18, −3 kV Distance 15 cm	DMF	PVP	Redox CO_2	300-W Xe light	8.08 $\mu mol\ g^{-1}\cdot h^{-1}$	Guo et al.[38]
CQDs-$Bi_{20}TiO_{32}$/PAN	Voltage 20 kV Distance 20 cm	DMAc	PAN	Degrading isoproturon	500-W Xe light Isoproturon solution at 15 mg/L	90.4% within 3 h	Xie et al.[39]
$Bi/Bi_xTiO\text{-}TiO_{yz2}$/CNFs	Voltage 25 kV Distance 15 cm	CH_3COOH, C_2H_5OH, DMF	PAN	Degrading RhB	300-W Xe light RhB solution at 10 mg/L	97% within 30 min	Yao et al.[40]
Cu^0/S-doped TiO_2	Voltage 18 kV Distance 15 cm	CH_3COOH, C_2H_5OH	PVP	Hydrogen production	Magnetic stirring under sunlight	91% within 90 min	Yousef et al.[41]
$Fe_2O_3\text{-}TiO_2$	Voltage 15 kV Distance 15 cm	DMF, CH_3COOH, C_2H_5O	PVP	Degrading CR	Congo red aqueous solution at 10 mg/L	78.8% within 90 min	Sheikh et al.[42]

OTC, oxytetracycline; DMAc, N,N-dimethylacetamide; CR, congo red.

recombination. This led to significant improvements in photocatalytic efficiency, with degradation rates of 27.2% for rhodamine B, 40.9% for methylene blue, and 31% for Cr(VI) within 60 min, far outperforming commercial TiO_2.

Wei Qi et al.[48] developed Zr/Ag co-doped TiO_2 nanofibers through electrospinning, creating a core-shell structure that optimized photocatalytic performance. Zr stabilized the anatase phase of TiO_2, while Ag nanoparticles provided plasmonic effects, extending light absorption into the visible range. The synergistic heterojunction between Zr and Ag further improved charge carrier mobility and electron-hole separation. This resulted in a 12-fold increase in the degradation rate constant for Congo red dye compared with undoped TiO_2.

Some studies have indicated that introducing dopants into the core or shell layer while constructing a heterojunction structure using coaxial electrospinning is a viable strategy to enhance the performance of the product. Sangmo Kang et al.[49] used this technique to fabricate Ag^+-doped rGO/TiO_2 core-shell nanofibers, which exhibited a 25-fold increase in the photocatalytic reduction of CO_2 to CH_4 compared with undoped TiO_2 nanofibers. This enhancement was due to Ag nanoparticles acting as electron traps, minimizing recombination, while the rGO layer facilitated rapid electron transport thanks to its high conductivity. The core-shell structure also provided a larger surface area for photon absorption and improved interaction with the reactants.

In a notable study by Zi Zhu et al.,[50] Ce-doped TiO_2/graphite/g-C_3N_4 heterojunctions were synthesized using a tri-coaxial electrospinning technique. This method allowed for the uniform incorporation of Ce into the TiO_2 matrix, resulting in a hybrid material with superior photocatalytic hydrogen evolution rates. The coaxial electrospinning process played a critical role in achieving the precise doping required for the efficient separation of photogenerated charge carriers, as well as optimizing the interaction between TiO_2, Ce, and the other components in the heterojunction. The polarization effect of the graphite layer further strengthened the internal electric field, enhancing charge transfer and suppressing recombination. The Ce-doped TiO_2 nanofibers prepared by electrospinning exhibited a remarkable hydrogen production rate, four times higher than that of undoped TiO_2, demonstrating the potential of this technique in producing high-performance photocatalytic materials.

The doping of different materials plays an important role in improving the photocatalytic performance, and a summary of related works by electrostatic spinning methods is presented in Table 3.

COMPOSITE CONSTRUCTION

Semiconductor photocatalysts with a wide band gap often face the challenge of limited light absorption, whereas those with a narrow band gap are prone to significant charge recombination. Constructing composite system is a feasible method for solving these problems.[62] Electrospinning technology can facilitate an *in situ* combination by simply mixing the raw materials into the spinning solution and can even produce a one-dimensional core-shell structure through coaxial spinning, which enhances the interaction between the composite materials, and thus has been widely researched.[63,64]

Table 3. Doping using electrostatic spinning

Photocatalyst	Spinning conditions	Solvents	Carrier polymers	Photocatalytic testing	Test conditions	Activity results	Reference
La-doped ZnO	Voltage 15 kV Distance 20 cm	DMF	PAN	Degrading RhB	350-W Xe light RhB solution at 10 mg/L	94.31% within 510 min	Jian et al.[46]
(N,F) co-doped $TiO_{2-\delta}$	Voltage 18 kV	DMF	PAN	Degrading MB	5-W LED light	40.9% within 60 min	Chen et al.[47]
Zr/Ag co-doped (TiO_2)	Voltage 15 kV Distance 12 cm	C_2H_5OH	PVP	Degrading CR	300-W Xe light CR solution at 30 mg/L	99.3% within 120 min	Qi et al.[48]
Ag/TiO_2	Voltage 15 kV Distance 8 cm	DMF, CH_3COOH	PVP	Redox CO_2	500-W Xe light	4.301 $\mu mol\ g^{-1}$ in 7 h	Kang et al.[49]
Ce-doped TiO_2/graphite/g-C_3N_4	–	DMF, C_2H_5OH	PVP	Hydrogen -production	300-W Xe light	3.05 $mmol\ g^{-1}\cdot h^{-1}$	Zhu et al.[50]
Sr-doped $Bi_4O_5Br_2/Bi_2MoO_6$	Voltage 20 kV Distance 18 cm	DMF	PAN	Degrading 4-CP	300-W visible LED light 4-CP solution at 10 mg/L	98.7% within 80 min	Pan et al.[51]
Fe-doped $LaMnO_3$	Voltage +12, −2 kV Distance 15 cm	DMF	PVP	Hydrogen production	300-W Xe light	767.71 $\mu mol\ g^{-1}\cdot h^{-1}$	Zhan et al.[52]
Sc-doped Bi_3TiNbO_9	Voltage 20 kV Distance 15 cm	C_2H_5OH, CH_3COOH	PVP	Degrading RhB	RhB solution at 20 mg/L	98.55% within 120 min	Song et al.[53]
C-ZnO	Voltage 15 kV Distance 15 cm	DMF	PAN	Degrading caffeine	300-W solar light Caffeine solution at 30 ppm	80.4% within 120 min	Gadisa et al.[54]
$Bi_{0.9}Gd_{0.07}La_{0.03}FeO_3$	Voltage 15 kV Distance 15 cm	DMF	PVP	Degrading MB	300-W Xe light MB solution at 20 mg/L	89% within 90 min	Mani et al.[55]
Ag/Fe-HAP@CA	Voltage 18 kV Distance 15 cm	CH_3COCH_3	CA	Degrading MB	MB solution at 10 mg/L	Over 90% within 2 h	Shalan et al.[56]
Fe-doped TiO_2	Voltage 20 kV Distance 20 cm	C_2H_5OH	PVP	Degrading MB	500-W Xe light MB solution at 20 mg/L	38.3% within 90 min	Na et al.[57]
Sn^{4+}-doped $BiFeO_3$	Voltage 17 kV Distance 14 cm	DMF	PAN	O_2 evolution	300-W Xe light	516.4 $mmol\ g^{-1}\cdot h^{-1}$	Ren et al.[58]
Fe-doped ZnO	Voltage 17.5 kV Distance 10 cm	DW	PVA	Degrading MB	50-W Xe light MB solution at 10 mg/L	Above 80% for 6 h	Liu et al.[59]
Ta-doped TiO_2	Voltage 13 kV	DI, C_2H_5OH	PVP	Degrading MB	12-W UV lamp MB solution at 20 μM	Above 90% for 4 h	Singh et al.[60]
N-doped In_2O_3	Voltage 10 kV Distance 10 cm	DMF	PVP	Degrading RhB	150-W Xe light RhB solution at 10 mg/L	97% within 180 min	Lu et al.[61]

LED, light-emitting diode.

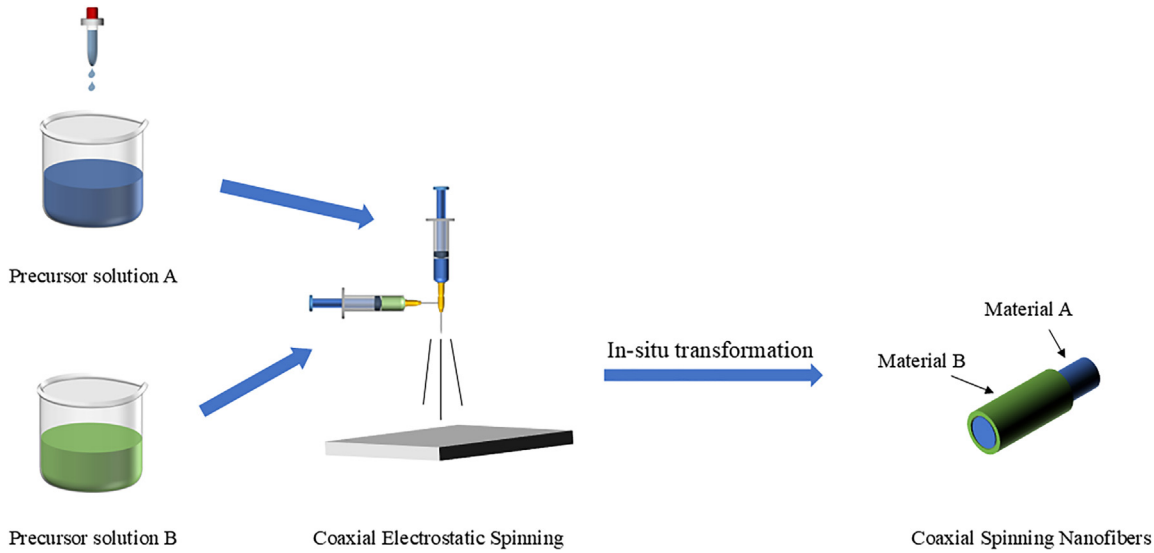

Figure 6. Coaxial electrostatically core-shell-structured nanofiber

Several studies have employed uniaxial electrospinning techniques to construct composite systems by modifying the spinning solution composition, highlighting the versatility of this method in enhancing photocatalytic performance. Yinyin Ai et al.[64,65] prepared a $ZnIn_2Se_4/TiO_2$ composite via electrospinning, featuring a Z-scheme heterojunction with $ZnIn_2Se_4$ nanoparticles tightly bonded to TiO_2 nanofibers through Ti-Se interfacial bonds. This strong interface, formed through uniaxial electrospinning, enhances the internal electric field, promoting efficient charge transfer and reducing electron-hole recombination. As a result, the composite achieved a photocatalytic hydrogen evolution rate of 0.11 mmol/g/h, three times higher than bare TiO_2. The Ti-Se bond and internal electric field make this structure particularly effective for hydrogen production and other catalytic applications. Beyond increasing surface area, electrospinning plays a crucial role in optimizing electron transport pathways, improving overall photocatalytic performance.

Similarly, QingHao Li and colleagues synthesized $CS/TiO_2/g\text{-}C_3N_4$ composite nanofibers via electrospinning,[66] achieving a Cr(VI) removal rate of over 90% under visible light, a 50% improvement over pure CS. The synergy between $g\text{-}C_3N_4$ and TiO_2 broadened light absorption and enhanced charge separation, key factors that improved the material's photocatalytic performance. The composite also maintained high stability and activity over multiple cycles, demonstrating the durability imparted by the electrospinning process, making it suitable for real-world applications.

Lu Wang et al.[67] used electrospinning to create $g\text{-}C_3N_4/Nb_2O_5$ composite nanofibers, resulting in a specific surface area of 36.18 $m^2\ g^{-1}$, 1.2 times higher than that of Nb_2O_5 alone. The heterojunction between $g\text{-}C_3N_4$ and Nb_2O_5 effectively reduced the band gap, extending light absorption into the visible spectrum and leading to an RhB degradation efficiency of 98.1% in two hours—nearly double that of Nb_2O_5 nanofibers. The increased surface area, combined with enhanced charge separation, underscores how electrospinning facilitates the creation of highly efficient catalytic materials by improving both structural and electronic properties.

In certain studies, composite fibers with core-shell structures have been constructed using coaxial spinning technology, in which the precursors of the materials are separately placed in the outer shell and inner core, as shown in the Figure 6. For instance, Yang Yaoyao et al.[68] prepared AgCl/ZnO-loaded nanofibrous membranes using coaxial electrospinning. The core-shell structure provided by the coaxial technique allowed for the separation of AgCl in the core and ZnO in the shell, enhancing the material's stability and active site exposure. This architecture facilitated efficient electron-hole separation and charge transport, resulting in a photocatalytic degradation efficiency of 98% for MB within 70 min, with over 95% efficiency retained across five cycles. The structural control offered by coaxial electrospinning was key in improving both the photocatalytic performance and long-term stability of the nanofibers.

Similarly, Mao Yihang et al.[69] developed $g\text{-}C_3N_4$/PAN/PANI@-$LaFeO_3$ core-shell nanofibrous membranes using coaxial electrospinning, where the core-shell design played a critical role in enhancing the photocatalytic properties. The $LaFeO_3$ was deposited in the outer shell, whereas $g\text{-}C_3N_4$ and PAN/PANI were distributed in the core, forming a Z-scheme heterojunction. This configuration promoted efficient charge separation, extended light absorption, and increased pollutant interaction with the active sites. As a result, the membranes achieved high pollutant removal rates, including 97.0% for MB, 94.3% for methyl violet, and 87.6% for ciprofloxacin. The structured design not only boosted photocatalytic efficiency but also ensured strong mechanical integrity and reusability.

In another example, Bin Jiang et al.[70] used coaxial electrospinning to synthesize SnO_2@PW12@TiO_2 core-shell nanofibers, forming a complex three-layer structure. The SnO_2 core, PW12 middle layer, and TiO_2 outer shell were strategically designed to create a Z-scheme heterojunction between the layers, which

Table 4. Compounding with electrostatic spinning

Photocatalyst	Spinning conditions	Solvents	Carrier polymers	Photocatalytic testing	Test conditions	Activity results	Reference
$ZnIn_2Se_4/TiO_2$	Voltage +15, −5 kV Distance 20 cm	CH_3COOH, C_2H_5OH	PVP	Hydrogen production	–	0.11 mmol $g^{-1}\cdot h^{-1}$	–
CS/g-C_3N_4/TiO_2	Voltage 15 kV Pushing speed 5 mL h^{-1}	CH_3COOH	PEO	Redox Cr(VI)	800-W Xe light Cr(VI) solution 100 mg/L	90% within 4 h	Li et al.[66]
g-C_3N_4/Nb_2O_5	Voltage 18 kV Distance 20 cm	DMF	PVP	Degrading RhB	–	98.1% within 120 min	Wang et al.[67]
AgCl/ZnO	Voltage 10 kV Distance 15 cm	C_2H_5OH, DI	PVP	Degrading MB	300-W Xe lamp	99.70% within 35 min	Yang et al.[68]
g-C_3N_4/PAN/PANI@$LaFeO_3$	Voltage 18 kV Distance 15 cm	DMF	PAN	Degrading MB	500-W Xe lamp MB solution at 20 mg/L	97% within 75 min	Mao et al.[69]
m-Hal@Ag_3PO_4/PAN	Voltage +18, −2 kV Distance 15 cm	DMF	PAN	Degrading ciprofloxacin	500-W Xe light Ciprofloxacin solution at 15 mg/L	99.98% within 200 min	Ma et al.[71]
SnO_2@PW_{12}@TiO_2	–	CH_3COOH, C_2H_5OH, DMF	PVP	Degrading TC	300-W Xe light TC solution at 20 mg/L	73.8% within 30 min	Jiang et al.[70]
NaYF4/Yb/Tm/TiO_2	–	C_2H_5OH, CH_3COOH	PVP	Degrading RhB	RhB solution at 0.01 mmol/L	99.12% within 2 h	Guo et al.[72]
TiO_2/WO_3	Voltage 15 kV Distance 8 cm Pushing speed 1 mL h^{-1}	CH_3COOH, C_2H_5OH	PVP	Degrading MO	UV and visible light MO solution was 4 × 10^{-5} M	21.6% within 240 min	Odhiambo et al.[73]
Fe_2O_3/TiO_2	Voltage 15 kV Distance 15 cm	CH_3COOH, C_2H_5OH	PVP	Degrading RhB	RhB solution 5 mg/L	99% within 90 min	Liu et al.[74]
$CoFe_2O_4$/BiOI	Voltage 12 kV Pushing speed 5 μL min^{-1}	DMF, C_2H_5OH	PVP	Degrading RhB	150- to 300-W Xe light RhB solution 10 mg/L	97.2% within 90 min	Chang et al.[75]
PAN/Bi_2MoO_6/Ti_3C_2	Voltage 20 kV Pushing speed 0.01 mm/s	DMF	PAN	Degrading tetracycline	300-W Xe light TC solution 15 mg/L	90.3% within 4 h	Zhang et al.[76]
TiO_2/WO_3/C/N	Voltage 20 kV Pushing speed 1 mL h^{-1}	CH_3COOH, C_2H_5OH	PVP	Degrading MB	MB solution 12.6 mg/L	39.4% within 4 h	Odhiambo et al.[77]
Au/CeO_2	Voltage 20 kV Pushing speed 0.5 mL h^{-1}	DMF	PVP	Degrading PhCHO	UV light	83.3% within 5 h	Li et al.[78]
g-$C_3N_4/K_{0.5}Na_{0.5}NbO_3$	Voltage 18 kV	C_2H_5OH	PVP	Hydrogen production	300-W Xe light	96.3 μmol $g^{-1}\cdot h^{-1}$	Zhang et al.[79]
$CuBi_2O_4/Bi_2O_3$	Voltage 18 kV Distance 12 cm	DMF	PVP	Degrading MO	–	99.2% within 130 min	Yang et al.[80]

(*Continued on next page*)

Table 4. *Continued*

Photocatalyst	Spinning conditions	Solvents	Carrier polymers	Photocatalytic testing	Test conditions	Activity results	Reference
$ZnIn_2S_4/Ag_2MoO_4$	Voltage 15 kV Distance 15 cm	DMF, C_2H_5OH, CH_3COOH	–	Degrading ENR	300-W Xe light ENR solution at 20 mg/L	100% within 120 min	Li et al.[81]
$ZnFe_2O_4$/Ag/AgBr	Voltage 17–19 kV	DMF	PVP	Degrading RhB	RhB solution at 100 mg/L	86.3% within 100 min	Sabzehmeidani et al.[82]
SiO_2/Ga_2O_3	Voltage 15 kV Distance 20 cm	DMF	PAN	Degrading RhB	RhB solution 10 mg/L	98% within 30 min	Du et al.[83]
$BN/Ce_2O_3/TiO_2$	Voltage 1.25 kV/cm Pushing speed 1 mL h^{-1}	C_2H_5OH	PVP	Hydrogen production	500-W halogen lamp	850 μmol $g^{-1}\cdot h^{-1}$	Ghorbanloo et al.[84]
$W_2N/C/TiO_{-n}$	Voltage 13 kV Distance 20 cm	DMF	PAN	Hydrogen production	300-W Xe light	3.11 μmol $g^{-1}\cdot h^{-1}$	Gong et al.[85]
$ZnO\text{-}In_2S_3$	Voltage 14 kV Distance 14 cm	DI	PVA	Hydrogen production	5-W blue LED	539.5 μmol $g^{-1}\cdot h^{-1}\cdot L^{-1}$	Chang et al.[86]
ZnO/Ti_3C_2	Voltage 14 kV Distance 14 cm	DMF	PVDF	Degrading CR	50-W LED light CR solution concentration 20 μM	96% within 210 min	Sahu and Dhar Purkayastha[87]
$Ni(DMG)_2/TiO_2$	Voltage 10 kV Distance 15 cm	DMF	PAN, PVP	Degrading MB	MB solution at 10 mg/L	97% within 60 min	Lv et al.[88]
$InVO_4/CeVO_4$	Voltage 20 kV Distance 20 cm	C_2H_5OH	PVP	Degrading TC	800-W Xe light TC solution at 20 mg/L	100% within 90 min	Ding et al.[89]
$WO_{2.72}/Fe_3O_4$	Voltage 15 kV Distance 15 cm	C_2H_5OH	PVA	Redox Cr(VI)	500-W Xe light	100% within 3 h	Motora et al.[90]
$WO_3/CdWO_4$	Voltage 20 kV Distance 15 cm	DMF, C_2H_5OH	PVP	Degrading TC	500-W Xe light TC solution at 10 mg/L	81.6% within 90 min	Rong et al.[91]
$PVDF/CdS/TiO_2$	Voltage 9.32 kV Distance 15 cm	DMF, CH_3COCH_3	PVDF	Redox Cr(VI)	350-W Xe light	96.6% within 40 min	Li et al.[92]
RGO/TiO_2/PANCMA	Voltage 14 kV Distance 30 cm	DMF	PANCMA	Degrading MG	MG solution at 100 ng/L	90.6% within 62 min	Du et al.[93]
$Rb_xWO_3@Fe_3O_4$	Voltage 15 kV Distance 15 cm	MC, DMF	PET	Redox Cr(VI)	Cr(VI) solution at 50 mg/L	100% within 90 min	Naseem et al.[94]
TiO_2(A-R)/$ZnTiO_3$	Voltage 18 kV Distance 18 cm	DMF	PVP	Hydrogen production	–	887.7 μmol $g^{-1}\cdot h^{-1}$	Yerli Soylu et al.[95]
$ZnO/ZnFe_2O_4$/Pt	Voltage 17 kV Pushing speed 0.5 mL h^{-1}	DMF	PVP	Degrading CIP	300-W Xe light CIP solution at 10 mg/L	92% within 2 h	Sobahi et al.[96]
$TiO_2\text{-}SiO_2\text{-}Al_2O_3\text{-}ZrO_2\text{-}CaO\text{-}CeO_2$	Voltage 20 kV Distance 13 cm	DMF	PAN	Degrading MB	MB solution at 20 mg/L	90.7% within 120 min	Yerli Soylu et al.[95]
$BiOI/SiO_2$	Voltage 9 kV Pushing speed 10 μL/min	DI	PVA	Degrading RhB	RhB solution 10 mg/L	68% within 3 h	Liu et al.[97]

(*Continued on next page*)

Table 4. *Continued*

Photocatalyst	Spinning conditions	Solvents	Carrier polymers	Photocatalytic testing	Test conditions	Activity results	Reference
CeO_2/CuS	Voltage 18–19 kV Pushing speed 0.05 mL/min	DMF, C_2H_5OH	PVP	Degrading MB	Striped blue LEDs MB solution 3 mg/L	96.38% within 50 min	Sabzehmeidani et al.[98]
ZnO/Ag	Voltage 28 kV Pushing speed 1.5 mL/h	DMF	PVP	Degrading MO	100-W UV lamp MB solution 10 mg/L	92% within 15 min	Li et al.[99]
$SrTiO_3$/TiO_2	Voltage 15 kV Distance 15 cm	DMF and CH_3COOH	PVP	Degrading MO	25-W UV-C mercury lamp MO solution at 15 mg/L	93% within 40 min	Zhao et al.[100]
ZnO/γ-Bi_2MoO_6	Voltage 20 kV Needle diameter 0.8 mm	DI and C_2H_5OH	PVP	Degrading MB	500-W Xe lamp	95.6% within 4 h	Wang et al.[101]
TiO_2@Ag@Cu_2O	Voltage 18 kV Needle Pushing speed 1.5 mL/h	DMF	PAN	Degrading MB	600-W Xe lamp MB solution at 10 mg/L	99% within 2.5 h	Li et al.[102]
Bi_2MoO_6/S-C_3N_4/PAN	Voltage 15 kV Pushing speed 0.5 mm/h	$C_2H_6O_2$, C_2H_5OH	PAN	Degrading 4-NP	An LED lamp (10-W, $\lambda \geq 400$ nm)	83% within 3 h	Chen et al.[103]
g-C_3N_4/AuNPs/PVDF	Voltage 20 kV Push speed 1.5 mL/h.	DI	PVDF	Degrading MB	Two COB LEDs	98% within 3 h	Saha et al.[104]
g-C_3N_4/BiOI	Voltage 10 kV Distance 16 cm	DMF	PAN	Degrading RhB	Visible light irradiation ($\lambda > 400$ nm)	98% within 90 min	Zhou et al.[105]
GO/MIL-101(Fe)/PANCMA	Voltage 11 kV Distance 30 cm	DMF	PAN	Degrading RhB	16-W UV lamp	93.7% within 20 min	Huang et al.[106]
$BaTiO_3$-TiO_2	Voltage 18kV Distance 15 cm	C_2H_5OH, CH_3COOH	PVP	Degrading RhB	300-W high pressure mercury lamp	99.8% within 1 h	Liu et al.[107]
Co_3O_4@CeO_2	Voltage 20 ± 0.5 kV	C_2H_5OH, CH_3COOH, DMF	PAN	Degrading levofloxacin	Levofloxacin concentration at 20 ppm	93.8% within 14 min	Wang et al.[108]
CuS QDs/$BiVO_4$@Y_2O_2S	Voltage 21 kV Distance 18 cm	DMF	PVP	Degrading RhB	300-W Xe lamp RhB solution at 10 mg/L	87.4% within 2 h	Guo et al.[109]
MoS_2/PANI/PAN@$BiFeO_3$	Voltage 17 kV Distance 15 cm	DMF	PAN, PANI	Degrading MO	MO solution 15 mg/L	99.9% within 60 min	Lin et al.[110]
Tm@ND@TiO_2/mSC	–	DMF	PAN/PEG	Degrading MO	MO solution 40 mg/L	94% within 60 min	Su et al.[111]
$CoMn_2O_4$/HACNFs	Voltage 13 kV Distance 8 cm	DMF	PMMA, PAN	Degrading RhB	RhB concentration at 50 μM	84.8% within 200 min	Kang et al.[112]

COB, chip-on-board; MO, methyl orange; ENR, enrofloxacin; PEO, polyethylene oxide; MC, methylene chloride; CIP, ciprofloxacin; PVDF, polyvinylidene fluoride; PEG, polyethylene glycol; PMMA, polymethyl methacrylate; PANCMA, poly(acrylonitrile-co-maleic acid); MG, malachite green.

enhanced charge separation and suppressed recombination. This multilayer structure increased the interaction between the active layers and maximized light absorption, leading to a 73.8% degradation of tetracycline within 30 min, compared with 44.8% for SnO_2@TiO_2 fibers without the PW12 layer. The enhanced photocatalytic performance was largely attributed to the efficient charge transfer pathways enabled by the core-shell architecture, highlighting the structural advantages coaxial electrospinning provides.

Electrostatic spinning is typically employed for the rapid fabrication of composite structures comprising diverse materials, as well as the synthesis of core-shell multilayered composite nanofibers. To facilitate rapid access to multilayered composites, we present a synopsis of composite precursor preparation methods and their catalytic activity in Table 4.

SUMMARY AND OUTLOOK

In recent years, electrospinning technology has found widespread application in the preparation of nanofiber-structured photocatalysts.[113] This review provides a comprehensive summary of the current application and development status of electrospinning technology in the preparation and modification of photocatalysts. Despite significant efforts, the industrial application of photocatalysis technology remains distant due to inadequate efficiency exhibited by current photocatalysts.[5] Constructing a multiple heterojunction compound model represents a potential strategy for designing highly active photocatalysts by enhancing charge separation properties.[114] However, the current methods, primarily wet-chemical and *in situ* growth, do not allow for precise arrangement of the components according to the model. In contrast, coaxial electrospinning technology is a suitable method for effectively constructing a multilayer system due to its ability to arrange materials in layers along the concentric axis. Therefore, the construction of a multicomponent composite system using coaxial electrospinning technology holds great significance for studying a multicomponent photocatalytic system model.

Moreover, electrospinning offers significant potential for large-scale production, particularly in fabricating complex nanostructures such as hollow, core-shell, and mesoporous fibers. These advanced architectures provide enhanced surface area and improved access to active catalytic sites, optimizing interactions between photocatalytic components and boosting reaction efficiency.[115] By facilitating better light absorption and charge transport pathways, electrospun nanofibers reduce electron-hole recombination, a key limitation in many photocatalytic systems. Understanding the process-structure-performance relationship—factors such as polymer composition, solution viscosity, applied voltage, and spinning speed—allows for fine-tuning fiber morphology, porosity, and crystallinity, all of which directly impact performance.[116] As electrospinning techniques evolve, they offer a scalable, cost-effective solution for producing high-performance photocatalysts, particularly in metal oxide semiconductor systems.[117] This approach not only enables industrial-scale production but also paves the way for advanced materials designed for environmental remediation, solar energy harvesting, and other energy applications.

ACKNOWLEDGMENTS

We are grateful for financial support from the National Natural Science Foundation of China (22002074), Natural Science Foundation of Shandong Province (ZR2022ME010), and Youth Innovation Team Program in Colleges of Shandong Province (2023KJ144).

AUTHOR CONTRIBUTIONS

Investigation and writing – original draft, F.G.; writing – review & editing, L.H., L.F., B.H., J.N., X.Z., S.C., and B.L.; supervision, X.Z. and S.C.

DECLARATION OF INTERESTS

The authors declare no competing interests.

REFERENCES

1. Baig, N., Kammakakam, I., and Falath, W. (2021). Nanomaterials: a review of synthesis methods, properties, recent progress, and challenges. Mater. Adv. *2*, 1821–1871. https://doi.org/10.1039/d0ma00807a.
2. Wu, X., Zhang, Q., Li, W., Qiao, B., Ma, D., and Wang, S.L. (2021). Atomic-scale Pd on 2D titania sheets for selective oxidation of methane to methanol. ACS Catal. *11*, 14038–14046. https://doi.org/10.1021/acscatal.1c03985.
3. Lakhani, P., Bhanderi, D., and Modi, C.K. (2024). Nanocatalysis: recent progress, mechanistic insights, and diverse applications. J. Nanoparticle Res. *26*, 148. https://doi.org/10.1007/s11051-024-06053-9.
4. Chen, X., Cao, H., He, Y., Zhou, Q., Li, Z., Wang, W., He, Y., Tao, G., and Hou, C. (2022). Advanced functional nanofibers: strategies to improve performance and expand functions. Front. Optoelectron. *15*, 50. https://doi.org/10.1007/s12200-022-00051-2.
5. Zhong, Y., Peng, C., He, Z., Chen, D., Jia, H., Zhang, J., Ding, H., and Wu, X. (2021). Interface engineering of heterojunction photocatalysts based on 1D nanomaterials. Catal. Sci. Technol. *11*, 27–42. https://doi.org/10.1039/d0cy01847c.
6. Yuan, S., and Zhang, Q. (2021). Application of one-dimensional nanomaterials in catalysis at the single-molecule and single-particle scale. Front. Chem. *9*, 812287. https://doi.org/10.3389/fchem.2021.812287.
7. Li, Y., Zhu, J., Cheng, H., Li, G., Cho, H., Jiang, M., Gao, Q., and Zhang, X. (2021). Developments of advanced electrospinning techniques: A critical review. Adv. Mater. Technol. *6*, 2100410. https://doi.org/10.1002/admt.202100410.
8. Islam, M.S., Ang, B.C., Andriyana, A., and Afifi, A.M. (2019). A review on fabrication of nanofibers via electrospinning and their applications. SN Appl. Sci. *1*, 1248. https://doi.org/10.1007/s42452-019-1288-4.
9. Chen, S., Zhou, J., Fang, B., Ying, Y., Yu, D., and He, H. (2023). Three EHDA processes from a detachable spinneret for fabricating drug fast dissolution composites. Macromol. Mater. Eng. *309*, 2300361. https://doi.org/10.1002/mame.202300361.
10. Chen, X., Liu, Y., and Liu, P. (2024). Electrospun core–sheath nanofibers with a cellulose acetate coating for the synergistic release of zinc ion and drugs. Mol. Pharm. *21*, 173–182. https://doi.org/10.1021/acs.molpharmaceut.3c00703.
11. Zhou, J., Chen, Y., Liu, Y., Huang, T., Xing, J., Ge, R., and Yu, D.G. (2024). Electrospun medicated gelatin/polycaprolactone Janus fibers for photothermal-chem combined therapy of liver cancer. Int. J. Biol. Macromol. *269*, 132113. https://doi.org/10.1016/j.ijbiomac.2024.132113.

12. Wang, M., Hou, J., Yu, D.G., Li, S., Zhu, J., and Chen, Z. (2020). Electrospun tri-layer nanodepots for sustained release of acyclovir. J. Alloys Compd. *846*, 156471. https://doi.org/10.1016/j.jallcom.2020.156471.

13. Xu, L., Li, Q., Wang, H., Liu, H., Yu, D.-G., Bligh, S.-W.A., and Lu, X. (2024). Electrospun multi-functional medicated tri-section Janus nanofibers for an improved anti-adhesion tendon repair. Chem. Eng. J. *492*, 152359. https://doi.org/10.1016/j.cej.2024.152359.

14. Sun, Y., Zhou, J., Zhang, Z., Yu, D.-G., and Bligh, S.W.A. (2024). Integrated Janus nanofibers enabled by a co-shell solvent for enhancing icariin delivery efficiency. Int. J. Pharm. *658*, 124180. https://doi.org/10.1016/j.ijpharm.2024.124180.

15. Yu, D.G., Gong, W., Zhou, J., Liu, Y., Zhu, Y., and Lu, X. (2024). Engineered shapes using electrohydrodynamic atomization for an improved drug delivery. WIREs Nanomed. Nanobiotechnol. *16*, e1964. https://doi.org/10.1002/wnan.1964.

16. Sun, L., Zhou, J., Chen, Y., Yu, D.-G., and Liu, P. (2023). A combined electrohydrodynamic atomization method for preparing nanofiber/microparticle hybrid medicines. Front. Bioeng. Biotechnol. *11*, 1308004. https://doi.org/10.3389/fbioe.2023.1308004.

17. Mao, H., Zhou, J., Yan, L., Zhang, S., and Yu, D.-G. (2024). Hybrid films loaded with 5-fluorouracil and Reglan for synergistic treatment of colon cancer via asynchronous dual-drug delivery. Front. Bioeng. Biotechnol. *12*, 1398730. https://doi.org/10.3389/fbioe.2024.1398730.

18. Zhang, P., Zhao, Y., Li, Y., Li, N., Silva, S.R.P., Shao, G., and Zhang, P. (2023). Revealing the selective bifunctional electrocatalytic sites via *in situ* irradiated x-ray photoelectron spectroscopy for lithium–sulfur battery. Adv. Sci. *10*, e2206786. https://doi.org/10.1002/advs.202206786.

19. Ahmadi Bonakdar, M., and Rodrigue, D. (2024). Electrospinning: processes, structures, and materials. Macromolecules (Washington, DC, U. S.) *4*, 58–103. https://doi.org/10.3390/macromol4010004.

20. Yoon, J., Yang, H.S., Lee, B.S., and Yu, W.R. (2018). Recent progress in coaxial electrospinning: New parameters, various structures, and wide applications. Adv. Mater. *30*, e1704765. https://doi.org/10.1002/adma.201704765.

21. Chen, Y.-F., Lee, Y.-C., Lee, J.C.-M., Li, J.-W., and Chiu, C.-W. (2024). Coaxial electrospinning of Au@silicate/poly(vinyl alcohol) core/shell composite nanofibers with non-covalently immobilized gold nanoparticles for preparing flexible, freestanding, and highly sensitive SERS substrates amenable to large-scale fabrication. Adv. Compos. Hybrid Mater. *7*, 124. https://doi.org/10.1007/s42114-024-00933-3.

22. Liu, R., Hou, L., Yue, G., Li, H., Zhang, J., Liu, J., Miao, B., Wang, N., Bai, J., Cui, Z., et al. (2022). Progress of fabrication and applications of electrospun hierarchically porous nanofibers. Adv. Fiber Mater. *4*, 604–630. https://doi.org/10.1007/s42765-022-00132-z.

23. Lu, J., Liu, M., Zhou, S., Zhou, X., and Yang, Y. (2017). Electrospinning fabrication of $ZnWO_4$ nanofibers and photocatalytic performance for organic dyes. Dyes Pigments *136*, 1–7. https://doi.org/10.1016/j.dyepig.2016.08.008.

24. Wang, L., Yang, G., Peng, S., Wang, J., Ji, D., Yan, W., and Ramakrishna, S. (2017). Fabrication of $MgTiO_3$ nanofibers by electrospinning and their photocatalytic water splitting activity. Int. J. Hydrogen Energy *42*, 25882–25890. https://doi.org/10.1016/j.ijhydene.2017.08.194.

25. Perween, S., and Ranjan, A. (2017). Improved visible-light photocatalytic activity in $ZnTiO_3$ nanopowder prepared by sol-electrospinning. Sol. Energy Mater. Sol. Cell. *163*, 148–156. https://doi.org/10.1016/j.solmat.2017.01.020.

26. Kim, J. (2022). Hollow TiO_2/Poly (Vinyl Pyrrolidone) fibers obtained via coaxial electrospinning as easy-to-handle photocatalysts for effective nitrogen oxide removal. Polymers *14*, 4942. https://doi.org/10.3390/polym14224942.

27. Li, S., Guo, M., Wang, X., and Gao, K. (2019). Fabrication and photocatalytic activity of $LaFeO_3$ ribbon-like nanofibers. J. Chin. Chem. Soc. *67*, 990–997. https://doi.org/10.1002/jccs.201900431.

28. Lv, C., Sun, J., Chen, G., Zhou, Y., Li, D., Wang, Z., and Zhao, B. (2017). Organic salt induced electrospinning gradient effect: Achievement of $BiVO_4$ nanotubes with promoted photocatalytic performance. Appl. Catal. B Environ. *208*, 14–21. https://doi.org/10.1016/j.apcatb.2017.02.058.

29. Pantò, F., Dahrouch, Z., Saha, A., Patanè, S., Santangelo, S., and Triolo, C. (2021). Photocatalytic degradation of methylene blue dye by porous zinc oxide nanofibers prepared via electrospinning: When defects become merits. Appl. Surf. Sci. *557*, 149830. https://doi.org/10.1016/j.apsusc.2021.149830.

30. Tong, H.x., Tian, X., Wu, D.x., Wang, C.f., Zhang, Q.l., and Jiang, Z.h. (2017). WO_3 nanofibers on ACF by electrospun for photo-degradation of phenol solution. J. Cent. South Univ. *24*, 1275–1280. https://doi.org/10.1007/s11771-017-3532-7.

31. Goodarzi, N., Ashrafi-Peyman, Z., Khani, E., and Moshfegh, A.Z. (2023). Recent progress on semiconductor heterogeneous photocatalysts in clean energy production and environmental remediation. Catalysts *13*, 1102. https://doi.org/10.3390/catal13071102.

32. Liu, J., Yao, H., Chai, X., Zhang, X., and Fu, J. (2024). Review of electrospinning technology of photocatalysis, electrocatalysis and magnetic response. J. Mater. Sci. *59*, 10623–10649. https://doi.org/10.1007/s10853-024-09788-x.

33. Zhang, J., Jiang, X., Huang, J., Lu, W., and Zhang, Z. (2022). Plasmon-enhanced photocatalytic overall water-splitting over Au nanoparticle-decorated $CaNb_2O_6$ electrospun nanofibers. J. Mater. Chem. A Mater. *10*, 20048–20058. https://doi.org/10.1039/d2ta05332b.

34. Han, C., Mao, W., Bao, K., Xie, H., Jia, Z., and Ye, L. (2017). Preparation of Ag/Ga_2O_3 nanofibers via electrospinning and enhanced photocatalytic hydrogen evolution. Int. J. Hydrogen Energy *42*, 19913–19919. https://doi.org/10.1016/j.ijhydene.2017.06.076.

35. Ye, S., Zhou, X., Xu, Y., Lai, W., Yan, K., Huang, L., Ling, J., and Zheng, L. (2019). Photocatalytic performance of multi-walled carbon nanotube/$BiVO_4$ synthesized by electro-spinning process and its degradation mechanisms on oxytetracycline. Chem. Eng. J. *373*, 880–890. https://doi.org/10.1016/j.cej.2019.05.109.

36. Jo, S., Kim, H., and Lee, T.S. (2021). Decoration of conjugated polyquinoxaline dots on mesoporous TiO_2 nanofibers for visible-light-driven photocatalysis. Polymer *228*, 123892. https://doi.org/10.1016/j.polymer.2021.123892.

37. Kumar, L., Singh, S., Horechyy, A., Formanek, P., Hübner, R., Albrecht, V., Weißpflog, J., Schwarz, S., Puneet, P., and Nandan, B. (2020). Hollow Au@TiO_2 porous electrospun nanofibers for catalytic applications. RSC Adv. *10*, 6592–6602. https://doi.org/10.1039/c9ra10487a.

38. Guo, X., Qiu, C., Zhang, Z., Zhang, J., Wang, L., Ding, J., Zhang, J., Wan, H., and Guan, G. (2024). Coaxial electrospinning prepared Cu species loaded $SrTiO_3$ for efficient photocatalytic reduction of CO_2 to CH_3OH. J. Environ. Chem. Eng. *12*, 111990. https://doi.org/10.1016/j.jece.2024.111990.

39. Xie, R., Zhang, L., Liu, H., Xu, H., Zhong, Y., Sui, X., and Mao, Z. (2017). Construction of CQDs-$Bi_{20}TiO_{32}$/PAN electrospun fiber membranes and their photocatalytic activity for isoproturon degradation under visible light. Mater. Res. Bull. *94*, 7–14. https://doi.org/10.1016/j.materresbull.2017.05.040.

40. Yao, L., Sun, C., Lin, H., Li, G., Lian, Z., Song, R., Zhuang, S., and Zhang, D. (2023). Electrospun Bi-decorated $Bi_xTi_yO_z$/TiO_2 flexible carbon nanofibers and their applications on degradating of organic pollutants under solar radiation. J. Mater. Sci. Technol. *150*, 114–123. https://doi.org/10.1016/j.jmst.2022.07.066.

41. Yousef, A., Brooks, R.M., El-Halwany, M.M., El-Newehy, M.H., Al-Deyab, S.S., and Barakat, N.A. (2016). Cu^0/S-doped TiO_2 nanoparticles-decorated carbon nanofibers as novel and efficient photocatalyst for hydrogen generation from ammonia borane. Ceram. Int. *42*, 1507–1512. https://doi.org/10.1016/j.ceramint.2015.09.097.

42. Sheikh, F.A., Appiah-Ntiamoah, R., Zargar, M.A., Chandradass, J., Chung, W.-J., and Kim, H. (2016). Photocatalytic properties of Fe_2O_3-modified rutile TiO_2 nanofibers formed by electrospinning technique. Mater. Chem. Phys. *172*, 62–68. https://doi.org/10.1016/j.matchemphys.2015.12.060.

43. Wang, W., Du, L., Xia, R., Liang, R., Zhou, T., Lee, H.K., Yan, Z., Luo, H., Shang, C., Phillips, D.L., and Guo, Z. (2023). In situprotonated-phosphorus interstitial doping induces long-lived shallow charge trapping in porous $C_{3-x}N_4$ photocatalysts for highly efficient H_2 generation. Energy Environ. Sci. *16*, 460–472. https://doi.org/10.1039/d2ee02680e.

44. Khlyustova, A., Sirotkin, N., Kusova, T., Kraev, A., Titov, V., and Agafonov, A. (2020). Doped TiO2: the effect of doping elements on photocatalytic activity. Mater. Adv. *1*, 1193–1201. https://doi.org/10.1039/d0ma00171f.

45. Li, Y., Zhu, G., Huang, H., Xu, M., Lu, T., and Pan, L. (2019). A N, S dual doping strategy via electrospinning to prepare hierarchically porous carbon polyhedra embedded carbon nanofibers for flexible supercapacitors. J. Mater. Chem. A Mater. *7*, 9040–9050. https://doi.org/10.1039/c8ta12246f.

46. Jian, S., Tian, Z., Hu, J., Zhang, K., Zhang, L., Duan, G., Yang, W., and Jiang, S. (2022). Enhanced visible light photocatalytic efficiency of La-doped ZnO nanofibers via electrospinning-calcination technology. Adv. Powder Mater. *1*, 100004. https://doi.org/10.1016/j.apmate.2021.09.004.

47. Chen, Y., Li, A., Fu, X., and Peng, Z. (2022). Electrospinning-based (N,F)-co-doped $TiO_{2-\delta}$ nanofibers: An excellent photocatalyst for degrading organic dyes and heavy metal ions under visible light. Mater. Chem. Phys. *291*, 126672. https://doi.org/10.1016/j.matchemphys.2022.126672.

48. Qi, W., Yang, Y., Du, J., Yang, J., Guo, L., and Zhao, L. (2021). Highly photocatalytic electrospun Zr/Ag Co-doped titanium dioxide nanofibers for degradation of dye. J. Colloid Interface Sci. *603*, 594–603. https://doi.org/10.1016/j.jcis.2021.06.109.

49. Kang, S., and Hwang, J. (2022). rGO-wrapped Ag-doped TiO_2 nanofibers for photocatalytic CO_2 reduction under visible light. J. Clean. Prod. *374*, 134022. https://doi.org/10.1016/j.jclepro.2022.134022.

50. Zhu, Z., Zhang, H., Teng, Y., Lin, X., Li, M., and Li, Y. (2023). Enhanced photocatalytic hydrogen evolution over Ce–TiO_2/graphite/g-C_3N_4 ternary S-scheme heterojunction. Surface. Interfac. *41*, 103160. https://doi.org/10.1016/j.surfin.2023.103160.

51. Pan, Q., Wang, J., Chen, H., Yin, P., Cheng, Q., Xiao, Z., Zhao, Y.-Z., and Liu, H.-B. (2023). Piezo-photocatalysis of Sr-doped $Bi_4O_5Br_2$/Bi_2MoO_6 composite nanofibers to simultaneously remove inorganic and organic contaminants. J. Water Proc. Eng. *56*, 104330. https://doi.org/10.1016/j.jwpe.2023.104330.

52. Zhan, M., Fang, M., Li, L., Zhao, Y., Yang, B., Min, X., Du, P., Liu, Y., Wu, X., and Huang, Z. (2023). Effect of Fe dopant on oxygen vacancy variation and enhanced photocatalysis hydrogen production of $LaMnO_3$ perovskite nanofibers. Mater. Sci. Semicond. Process. *166*, 107697. https://doi.org/10.1016/j.mssp.2023.107697.

53. Song, Z., Yu, S., Wang, K., Jiang, Z., Xue, L., and Yang, F. (2023). Novel Sc-doped Bi_3TiNbO_9 ferroelectric nanofibers prepared by electrospinning for visible-light photocatalysis. J. Rare Earths *41*, 365–373. https://doi.org/10.1016/j.jre.2022.01.010.

54. Gadisa, B.T., Kassahun, S.K., AppiahNtiamoah, R., and Kim, H. (2020). Tuning the charge carrier density and exciton pair separation in electrospun 1D ZnO-C composite nanofibers and its effect on photodegradation of emerging contaminants. J. Colloid Interface Sci. *570*, 251–263. https://doi.org/10.1016/j.jcis.2020.03.002.

55. Mani, A.D., Li, J., Wang, Z., Zhou, J., Xiang, H., Zhao, J., Deng, L., Yang, H., and Yao, L. (2022). Coupling of piezocatalysis and photocatalysis for efficient degradation of methylene blue by $Bi_{0.9}Gd_{0.07}La_{0.03}FeO_3$ nanotubes. J. Adv. Ceram. *11*, 1069–1081. https://doi.org/10.1007/s40145-022-0590-6.

56. Shalan, A.E., Afifi, M., El-Desoky, M.M., and Ahmed, M.K. (2021). Electrospun nanofibrous membranes of cellulose acetate containing hydroxyapatite co-doped with Ag/Fe: morphological features, antibacterial activity and degradation of methylene blue in aqueous solution. New J. Chem. *45*, 9212–9220. https://doi.org/10.1039/d1nj00569c.

57. Na, K.H., Kim, B.S., Yoon, H.S., Song, T.H., Kim, S.W., Cho, C.H., and Choi, W.Y. (2021). Fabrication and photocatalytic properties of electrospun Fe-Doped TiO_2 nanofibers using polyvinyl pyrrolidone precursors. Polymers *13*, 2634. https://doi.org/10.3390/polym13162634.

58. Ren, J., Zhao, D., Liu, H., Zhong, Y., Ning, J., Zhang, Z., Zheng, C., and Hu, Y. (2018). Electrospinning preparation of Sn^{4+}-doped $BiFeO_3$ nanofibers as efficient visible-light-driven photocatalyst for O_2 evolution. J. Alloys Compd. *766*, 274–283. https://doi.org/10.1016/j.jallcom.2018.06.329.

59. Liu, L., Liu, Z., Yang, Y., Geng, M., Zou, Y., Shahzad, M.B., Dai, Y., and Qi, Y. (2018). Photocatalytic properties of Fe-doped ZnO electrospun nanofibers. Ceram. Int. *44*, 19998–20005. https://doi.org/10.1016/j.ceramint.2018.07.268.

60. Singh, N., Prakash, J., Misra, M., Sharma, A., and Gupta, R.K. (2017). Dual functional Ta-Doped electrospun TiO_2 nanofibers with enhanced photocatalysis and SERS detection for organic compounds. ACS Appl. Mater. Interfaces *9*, 28495–28507. https://doi.org/10.1021/acsami.7b07571.

61. Lu, N., Shao, C., Li, X., Miao, F., Wang, K., and Liu, Y. (2017). A facile fabrication of nitrogen-doped electrospun In_2O_3 nanofibers with improved visible-light photocatalytic activity. Appl. Surf. Sci. *391*, 668–676. https://doi.org/10.1016/j.apsusc.2016.07.057.

62. Wei, S., Wang, L., Yue, J., Wu, R., Fang, Z., and Xu, Y. (2023). Recent progress in polymer nanosheets for photocatalysis. J. Mater. Chem. A Mater. *11*, 23720–23741. https://doi.org/10.1039/d3ta05435g.

63. Meng, X., Qiao, J., Liu, J., Wu, L., Wang, Z., and Wang, F. (2024). Core–shell nanofibers/polyurethane composites obtained through electrospinning for ultra-broadband electromagnetic wave absorption. Adv. Compos. Hybrid Mater. *7*, 149. https://doi.org/10.1007/s42114-024-00976-6.

64. Jiang, X., Huang, J., Bi, Z., Ni, W., Gurzadyan, G., Zhu, Y., and Zhang, Z. (2022). Plasmonic active "hot spots"-confined photocatalytic CO_2 reduction with high selectivity for CH_4 production. Adv. Mater. *34*, e2109330. https://doi.org/10.1002/adma.202109330.

65. Ai, Y., Li, Y., Li, T., Hou, R., Wang, Q., Habib, A., Shao, G., and Zhang, P. (2024). $ZnIn_2Se_4$ nanoparticles photocatalyst for efficient solar fuel production. iScience *27*, 110422. https://doi.org/10.1016/j.isci.2024.110422.

66. Li, Q.H., Dong, M., Li, R., Cui, Y.Q., Xie, G.X., Wang, X.X., and Long, Y.Z. (2021). Enhancement of Cr(VI) removal efficiency via adsorption/photocatalysis synergy using electrospun chitosan/g-C_3N_4/TiO_2 nanofibers. Carbohydr. Polym. *253*, 117200. https://doi.org/10.1016/j.carbpol.2020.117200.

67. Wang, L., Li, Y., and Han, P. (2021). Electrospinning preparation of g-C_3N_4/Nb_2O_5 nanofibers heterojunction for enhanced photocatalytic degradation of organic pollutants in water. Sci. Rep. *11*, 22950. https://doi.org/10.1038/s41598-021-02161-x.

68. Yang, Y., Zhou, S., Cao, X., Lv, H., Liang, Z., Zhang, R., Ye, F., and Yu, D. (2024). Coaxial electrospun porous core–shell nanofibrous membranes for photodegradation of organic dyes. Polymers *16*, 754. https://doi.org/10.3390/polym16060754.

69. Mao, Y., Lin, L., Chen, Y., Yang, M., Zhang, L., Dai, X., He, Q., Jiang, Y., Chen, H., Liao, J., et al. (2023). Preparation of site-specific Z-scheme g-C_3N_4/PAN/PANI@$LaFeO_3$ cable nanofiber membranes by coaxial electrospinning: Enhancing filtration and photocatalysis performance. Chemosphere *328*, 138553. https://doi.org/10.1016/j.chemosphere.2023.138553.

70. Jiang, B., Wang, T., Li, F., Li, D., Yang, Y., Yu, H., and Dong, X. (2023). Polyoxometalate as pivotal interface in SnO_2@PW_{12}@TiO_2 coaxial nanofibers: From heterojunction design to photocatalytic and gas sensing

applications. Sensor. Actuator. B Chem. *390*, 133928. https://doi.org/10.1016/j.snb.2023.133928.

71. Ma, J., Jin, X., Lu, Y., Yang, M., Zhao, X., Guo, M., Zhang, H., Li, X., and Wang, B. (2024). Preparation of modified halloysite nanotubes@Ag_3PO_4/polyacrylonitrile electrospinning membranes for highly efficient air filtration and disinfection. Appl. Clay Sci. *253*, 107361. https://doi.org/10.1016/j.clay.2024.107361.
72. Guo, F., Guo, Z., Gao, L., Qi, D., Yue, G., Wang, N., Zhao, Y., Li, N., Xiong, J., and Low, J. (2021). Electrospun core-shell hollow structure cocatalysts for enhanced photocatalytic activity. J. Nanomater. *2021*, 1–7. https://doi.org/10.1155/2021/9980810.
73. Odhiambo, V.O., Ongarbayeva, A., Kéri, O., Simon, L., and Szilágyi, I.M. (2020). Synthesis of TiO_2/WO_3 composite nanofibers by a water-based electrospinning process and their application in photocatalysis. Nanomaterials *10*, 882. https://doi.org/10.3390/nano10050882.
74. Liu, H., Zhang, Z.G., Wang, X.X., Nie, G.D., Zhang, J., Zhang, S.X., Cao, N., Yan, S.Y., and Long, Y.Z. (2018). Highly flexible Fe_2O_3/TiO_2 composite nanofibers for photocatalysis and ultraviolet detection. J. Phys. Chem. Solid. *121*, 236–246. https://doi.org/10.1016/j.jpcs.2018.05.019.
75. Chang, M.J., Cui, W.N., Wang, H., Liu, J., Li, H.L., Du, H.L., and Peng, L.G. (2019). Recoverable magnetic $CoFe_2O_4$/BiOI nanofibers for efficient visible light photocatalysis. Colloids Surf. A Physicochem. Eng. Asp. *562*, 127–135. https://doi.org/10.1016/j.colsurfa.2018.11.016.
76. Zhang, J.J., Kai, C.M., Zhang, F.J., and Wang, Y.R. (2022). Novel PAN/Bi_2MoO_6/Ti_3C_2 ternary composite membrane via electrospinning with enhanced photocatalytic degradation of tetracycline. Colloids Surf. A Physicochem. Eng. Asp. *648*, 129255. https://doi.org/10.1016/j.colsurfa.2022.129255.
77. Odhiambo, V.O., Mustafa, C.R.M., Thong, L.B., Kónya, Z., Cserháti, C., Erdélyi, Z., Lukác, I.E., and Szilágyi, I.M. (2021). Preparation of TiO_2/WO_3/C/N composite nanofibers by electrospinning using precursors soluble in water and their photocatalytic activity in visible light. Nanomaterials *11*, 351. https://doi.org/10.3390/nano11020351.
78. Li, B., Zhang, B., Nie, S., Shao, L., and Hu, L. (2017). Optimization of plasmon-induced photocatalysis in electrospun Au/CeO_2 hybrid nanofibers for selective oxidation of benzyl alcohol. J. Catal. *348*, 256–264. https://doi.org/10.1016/j.jcat.2016.12.025.
79. Zhang, T., Chen, L., Yuan, C., Su, M., Liu, X., Huang, S., Jiang, M., Su, K., and Wang, D. (2023). The photocatalytic hydrogen evolution of g–C_3N_4/$K_{0.5}Na_{0.5}NbO_3$ nanofibers heterojunction under visible light. J. Photochem. Photobiol. Chem. *435*, 114192. https://doi.org/10.1016/j.jphotochem.2022.114192.
80. Yang, F., Yu, X., Liu, Z., Niu, J., Zhang, T., Nie, J., Zhao, N., Li, J., and Yao, B. (2021). Preparation of Z-scheme $CuBi_2O_4$/Bi_2O_3 nanocomposites using electrospinning and their enhanced photocatalytic performance. Mater. Today Commun. *26*, 101735. https://doi.org/10.1016/j.mtcomm.2020.101735.
81. Li, S., Dong, Z., Wang, Q., Zhou, X., Shen, L., Li, H., and Shi, W. (2022). Antibacterial Z-scheme $ZnIn_2S_4$/Ag_2MoO_4 composite photocatalytic nanofibers with enhanced photocatalytic performance under visible light. Chemosphere *308*, 136386. https://doi.org/10.1016/j.chemosphere.2022.136386.
82. Sabzehmeidani, M.M., Karimi, H., Ghaedi, M., and Avargani, V.M. (2021). Construction of efficient and stable ternary $ZnFe_2O_4$/Ag/AgBr Z-scheme photocatalyst based on $ZnFe_2O_4$ nanofibers under LED visible light. Mater. Res. Bull. *143*, 111449. https://doi.org/10.1016/j.materresbull.2021.111449.
83. Du, F., Yang, D., Kang, T., Ren, Y., Hu, P., Song, J., Teng, F., and Fan, H. (2022). SiO_2/Ga_2O_3 nanocomposite for highly efficient selective removal of cationic organic pollutant via synergistic electrostatic adsorption and photocatalysis. Separ. Purif. Technol. *295*, 121221. https://doi.org/10.1016/j.seppur.2022.121221.
84. Ghorbanloo, M., Nada, A.A., El-Maghrabi, H.H., Bekheet, M.F., Riedel, W., Djamel, B., Viter, R., Roualdes, S., Soliman, F.S., Moustafa, Y.M., et al. (2022). Superior efficiency of BN/Ce_2O_3/TiO_2 nanofibers for photocatalytic hydrogen generation reactions. Appl. Surf. Sci. *594*, 153438. https://doi.org/10.1016/j.apsusc.2022.153438.
85. Gong, S., Fan, J., Cecen, V., Huang, C., Min, Y., Xu, Q., and Li, H. (2021). Noble-metal and cocatalyst free W_2N/C/TiO photocatalysts for efficient photocatalytic overall water splitting in visible and near-infrared light regions. Chem. Eng. J. *405*, 126913. https://doi.org/10.1016/j.cej.2020.126913.
86. Chang, Y.C., Syu, S.Y., and Wu, Z.Y. (2021). Fabrication of ZnO-In_2S_3 composite nanofiber as highly efficient hydrogen evolution photocatalyst. Mater. Lett. *302*, 130435. https://doi.org/10.1016/j.matlet.2021.130435.
87. Sahu, S., and Dhar Purkayastha, D. (2023). 1D/2D ZnO nanoneedles/Ti_3C_2 MXene enrobed PVDF electrospun membrane for effective water purification. Appl. Surf. Sci. *622*, 156905. https://doi.org/10.1016/j.apsusc.2023.156905.
88. Lv, H., Zhang, M., Wang, P., Xu, X., Liu, Y., and Yu, D.-G. (2022). Ingenious construction of Ni$(DMG)_2$/TiO_2-decorated porous nanofibers for the highly efficient photodegradation of pollutants in water. Colloids Surf. A Physicochem. Eng. Asp. *650*, 129561. https://doi.org/10.1016/j.colsurfa.2022.129561.
89. Ding, W., Lin, X., Ma, G., and Lu, Q. (2020). Designed formation of $InVO_4$/$CeVO_4$ hollow nanobelts with Z-scheme charge transfer: Synergistically boosting visible-light-driven photocatalytic degradation of tetracycline. J. Environ. Chem. Eng. *8*, 104588. https://doi.org/10.1016/j.jece.2020.104588.
90. Motora, K.G., Wu, C.-M., and Naseem, S. (2021). Magnetic recyclable self-floating solar light-driven $WO_{2.72}$/Fe_3O_4 nanocomposites immobilized by Janus membrane for photocatalysis of inorganic and organic pollutants. J. Ind. Eng. Chem. *102*, 25–34. https://doi.org/10.1016/j.jiec.2021.06.025.
91. Rong, F., Lu, Q., Mai, H., Chen, D., and Caruso, R.A. (2021). Hierarchically porous WO_3/$CdWO_4$ fiber-in-tube nanostructures featuring readily accessible active sites and enhanced photocatalytic effectiveness for antibiotic degradation in water. ACS Appl. Mater. Interfaces *13*, 21138–21148. https://doi.org/10.1021/acsami.0c22825.
92. Li, W., Liao, G., Duan, W., Gao, F., Wang, Y., Cui, R., Wang, X., and Wang, C. (2024). Synergistically electronic interacted PVDF/CdS/TiO_2 organic-inorganic photocatalytic membrane for multi-field driven panel wastewater purification. Appl. Catal. B: Environ. Energy *354*, 124108. https://doi.org/10.1016/j.apcatb.2024.124108.
93. Du, F., Sun, L., Huang, Z., Chen, Z., Xu, Z., Ruan, G., and Zhao, C. (2020). Electrospun reduced graphene oxide/TiO_2/poly(acrylonitrile-co-maleic acid) composite nanofibers for efficient adsorption and photocatalytic removal of malachite green and leucomalachite green. Chemosphere *239*, 124764. https://doi.org/10.1016/j.chemosphere.2019.124764.
94. Naseem, S., Wu, C.-M., and Motora, K.G. (2021). Novel multifunctional Rb_xWO_3@Fe_3O_4 immobilized Janus membranes for desalination and synergic-photocatalytic water purification. Desalination *517*, 115256. https://doi.org/10.1016/j.desal.2021.115256.
95. Yerli Soylu, N., Soylu, A., Dikmetas, D.N., Karbancioglu Guler, F., Kucukbayrak, S., and Erol Taygun, M. (2023). Photocatalytic and antimicrobial properties of electrospun TiO_2–SiO_2–Al_2O_3–ZrO_2–CaO–CeO_2 ceramic membranes. ACS Omega *8*, 10836–10850. https://doi.org/10.1021/acsomega.2c06986.
96. Sobahi, T.R., and Amin, M.S. (2020). Synthesis of ZnO/$ZnFe_2O_4$/Pt nanoparticles heterojunction photocatalysts with superior photocatalytic activity. Ceram. Int. *46*, 3558–3564. https://doi.org/10.1016/j.ceramint.2019.10.073.
97. Liu, J., Chang, M.J., and Du, H.L. (2017). Fabrication and photocatalytic properties of flexible BiOI/SiO_2 hybrid membrane by electrospinning method. J. Nanosci. Nanotechnol. *17*, 3792–3797. https://doi.org/10.1166/jnn.2017.14008.

98. Sabzehmeidani, M.M., Karimi, H., and Ghaedi, M. (2019). Visible light-induced photo-degradation of methylene blue by n–p heterojunction CeO_2/CuS composite based on ribbon-like CeO_2 nanofibers via electrospinning. Polyhedron *170*, 160–171. https://doi.org/10.1016/j.poly.2019.05.040.

99. Li, Z., Fan, X., Meng, A., Zhang, Y., Zhu, K., and Li, Q. (2019). Porous nanofibers formed by heterogeneous growth of ZnO/Ag particles and the enhanced photocatalysis. J. Nanosci. Nanotechnol. *19*, 7163–7168. https://doi.org/10.1166/jnn.2019.16518.

100. Zhao, W., Zhang, J., Pan, J., Qiu, J., Niu, J., and Li, C. (2017). One-step electrospinning route of $SrTiO_3$-modified Rutile TiO_2 nanofibers and its photocatalytic properties. Nanoscale Res. Lett. *12*, 371. https://doi.org/10.1186/s11671-017-2130-9.

101. Wang, Q., Lu, Q., Wei, M., Guo, E., Yao, L., and Sun, K. (2017). ZnO/γ-Bi_2MoO_6 heterostructured nanotubes: electrospinning fabrication and highly enhanced photoelectrocatalytic properties under visible-light irradiation. J. Sol. Gel Sci. Technol. *85*, 84–92. https://doi.org/10.1007/s10971-017-4519-4.

102. Li, X., Raza, S., and Liu, C. (2021). Directly electrospinning synthesized Z-scheme heterojunction TiO_2@Ag@Cu_2O nanofibers with enhanced photocatalytic degradation activity under solar light irradiation. J. Environ. Chem. Eng. *9*, 106133. https://doi.org/10.1016/j.jece.2021.106133.

103. Chen, G., Hing Wong, N., Sunarso, J., Wang, Y., Liu, Z., Chen, D., Wang, D., and Dai, G. (2023). Flexible Bi_2MoO_6/S-C_3N_4/PAN heterojunction nanofibers made from electrospinning and solvothermal route for boosting visible-light photocatalytic performance. Appl. Surf. Sci. *612*, 155893. https://doi.org/10.1016/j.apsusc.2022.155893.

104. Saha, D., Gismondi, P., Kolasinski, K.W., Shumlas, S.L., Rangan, S., Eslami, B., McConnell, A., Bui, T., and Cunfer, K. (2021). Fabrication of electrospun nanofiber composite of g-C_3N_4 and Au nanoparticles as plasmonic photocatalyst. Surface. Interfac. *26*, 101367. https://doi.org/10.1016/j.surfin.2021.101367.

105. Zhou, X., Shao, C., Yang, S., Li, X., Guo, X., Wang, X., Li, X., and Liu, Y. (2018). Heterojunction of g-C_3N_4/BiOI immobilized on flexible electrospun polyacrylonitrile nanofibers: facile preparation and enhanced visible photocatalytic activity for floating photocatalysis. ACS Sustain. Chem. Eng. *6*, 2316–2323. https://doi.org/10.1021/acssuschemeng.7b03760.

106. Huang, Z., Lai, Z., Zhu, D., Wang, H., Zhao, C., Ruan, G., and Du, F. (2021). Electrospun graphene oxide/MIL-101(Fe)/poly(acrylonitrile-co-maleic acid) nanofiber: A high-efficient and reusable integrated photocatalytic adsorbents for removal of dye pollutant from water samples. J. Colloid Interface Sci. *597*, 196–205. https://doi.org/10.1016/j.jcis.2021.04.020.

107. Liu, Z., Zhao, K., Xing, G., Zheng, W., and Tang, Y. (2021). One-step synthesis of unique thorn-like $BaTiO_3$–TiO_2 composite nanofibers to enhance piezo-photocatalysis performance. Ceram. Int. *47*, 7278–7284. https://doi.org/10.1016/j.ceramint.2020.11.017.

108. Wang, D., Ding, S., He, Z., Zhang, T., and Wang, X. (2024). Tailor-made Co_3O_4@CeO_2 based nanofibrous membrane with enhanced catalytic reactivity for efficient degradation of antibiotic. Compos. B Eng. *278*, 111424. https://doi.org/10.1016/j.compositesb.2024.111424.

109. Guo, D., Jiang, S., Shen, L., Pun, E.Y.B., and Lin, H. (2024). Heterogeneous CuS QDs/$BiVO_4$@Y_2O_2S Nanoreactor for Monitorable Photocatalysis. Small *20*, 2401335. https://doi.org/10.1002/smll.202401335.

110. Lin, L., He, Q., Chen, Y., Wang, B., Zhang, L., Dai, X., Jiang, Y., Chen, H., Liao, J., Mao, Y., et al. (2023). MoS_2/polyaniline (PANI)/polyacrylonitrile (PAN)@$BiFeO_3$ bilayer hollow nanofiber membrane: Photocatalytic filtration and piezoelectric effect enhancing degradation and disinfection. J. Colloid Interface Sci. *644*, 29–41. https://doi.org/10.1016/j.jcis.2023.04.069.

111. Su, Y., Liu, L., and Wen, S. (2021). Broadband $NaYF_4$:Yb,Tm@$NaYF_4$:Yb,Nd@TiO_2 nanoparticles anchored on SiO_2/Carbon electrospun fibers for photocatalytic degradation of organic pollutants. ACS Appl. Nano Mater. *4*, 12576–12587. https://doi.org/10.1021/acsanm.1c03091.

112. Kang, S., and Hwang, J. (2021). $CoMn_2O_4$ embedded hollow activated carbon nanofibers as a novel peroxymonosulfate activator. Chem. Eng. J. *406*, 127158. https://doi.org/10.1016/j.cej.2020.127158.

113. Nadaf, A., Gupta, A., Hasan, N., Fauziya, Ahmad, S., Kesharwani, P., and Ahmad, F.J. (2022). Recent update on electrospinning and electrospun nanofibers: current trends and their applications. RSC Adv. *12*, 23808–23828. https://doi.org/10.1039/d2ra02864f.

114. Xia, M., Zhao, X., Zhang, Y., Pan, W., and Leung, D.Y.C. (2022). Rational catalyst design for spatial separation of charge carriers in a multi-component photocatalyst for effective hydrogen evolution. J. Mater. Chem. A Mater. *10*, 25380–25405. https://doi.org/10.1039/d2ta06609b.

115. Zhang, Z., Liu, H., Yu, D.G., and Bligh, S.W.A. (2024). Alginate-based electrospun nanofibers and the enabled drug controlled release profiles: A review. Biomolecules *14*, 789. https://doi.org/10.3390/biom14070789.

116. Ji, Y., Zhao, H., Liu, H., Zhao, P., and Yu, D.G. (2023). Electrosprayed stearic-acid-coated ethylcellulose microparticles for an improved sustained release of anticancer drug. Gels *9*, 700. https://doi.org/10.3390/gels9090700.

117. Zhao, P., Zhou, K., Xia, Y., Qian, C., Yu, D.G., Xie, Y., and Liao, Y. (2024). Electrospun trilayer eccentric Janus nanofibers for a combined treatment of periodontitis. Adv. Fiber Mater. *6*, 1053–1073. https://doi.org/10.1007/s42765-024-00397-6.